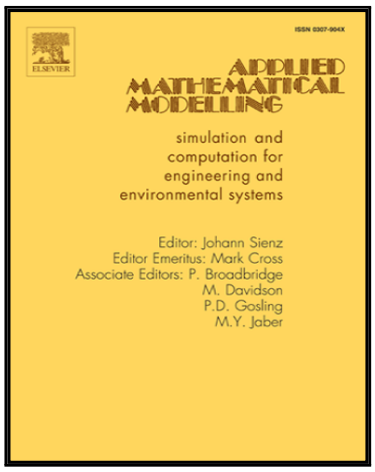

A novel mathematical formulation for predicting symmetric passive bipedal walking motion with unbalanced masses

P. Mahmoodi , R.S. Ransing , M.I. Friswell

PII: S0307-904X(15)00715-5
DOI: 10.1016/j.apm.2015.10.051
Reference: APM 10865

To appear in: *Applied Mathematical Modelling*

Received date: 23 September 2014
Revised date: 10 June 2015
Accepted date: 28 October 2015

Please cite this article as: P. Mahmoodi , R.S. Ransing , M.I. Friswell , A novel mathematical formulation for predicting symmetric passive bipedal walking motion with unbalanced masses, *Applied Mathematical Modelling* (2015), doi: 10.1016/j.apm.2015.10.051

Highlights:

1. A bipedal walking algorithm is presented for curved feet and unequal masses
2. The effect of changing length/mass ratio's on stable walking process is studied
3. Results are expressed in terms of roll-over shape curvature and foot length values
4. The new insights are useful in the design of prosthetic as well as robotic feet.

A novel mathematical formulation for predicting symmetric passive bipedal walking motion with unbalanced masses

P. Mahmoodi, R.S. Ransing[1], M.I. Friswell

College of Engineering, Swansea University, Swansea SA2 8PP, UK

[1]Corresponding author

Tel: +44(0) 1792 295219

Fax: +44(0)1792295676

Email: r.s.ransing@swansea.ac.uk

Abstract

Commercial prosthetic feet weigh about 25% of their equivalent physiological counterparts. The human body is able to overcome the walking asymmetry resulting from this mass imbalance by exerting more energy. It is hypothesised that the passive walking dynamics coupled with roll-over shapes has potential to suggest energy efficient walking solutions. A two link passive walking kinematic model has been proposed to study the gait pattern with unbalanced leg masses. An optimal roll-over shape for the prosthetic foot that minimises the asymmetry in the inter-leg angle and the step period is determined. The proposed mathematical formulation provides insights into the variation of step length and inter-leg angle with respect to the position and location of the centres for mass of both prosthetic and physiological legs.

Keywords: Gait analysis, Bifurcation diagrams, Chaos, Phase plane limit cycle, Passive bipedal model, Transtibial amputees, Prosthetic foot.

A novel mathematical formulation for predicting symmetric passive bipedal walking motion with unbalanced masses

List of Nomenclature

Parameters	Descriptions	Parameters	Descriptions
θ_s	Angle of stance leg	l_{vs}	Length virtual stance leg
θ_{vs}	Angle of virtual stance leg	a_{vs}	Length virtual stance lower leg
θ_{vsl}	Angle of virtual stance lower leg	m_H	Mass of hip joint
θ_{ns}	Angle of swing leg	m_s	Mass of stance leg
φ	Slope angle	m_{ns}	Mass of swing leg
μ	$\frac{m_H}{m_{physiological\ leg}}$	υ	$\frac{m_{prosthetideg}}{m_{physiologicalleg}}$
β	$\frac{\text{Physiological upperleg length}}{\text{Physiological lower leg length}}$	γ	$\frac{\text{Prosthetic upperleg length}}{\text{Physiological upperleg length}}$

1. Introduction

A prosthetic leg is an artificial limb and effectively is a dead weight. It is not supported by human muscles and the associated nervous system. Some of the commercially available prosthetic feet weigh only a quarter of the corresponding weight of the human leg. This paper investigates whether this mass imbalance has an influence on the kinematics of the gait. This is important as the human desire to maintain a symmetric walking gait irrespective of imbalances may increase energy consumption. Many gait descriptors have been presented to study the asymmetry of walking with a prosthetic foot [1, 2]. However, they did not include roll-over shapes. The roll-over shape is the locus of the centre of pressure as the foot rolls over the surface. It is defined in a local co-ordinate system with the *y* axis

aligned to the ankle-knee axis. The roll-over shape has been widely used to understand the knee-ankle-foot kinematics as it is invariant to many gait parameters such as added weight, speed and shoe heel height [3-5]. The ideal roll-over shape for the prosthetic foot may be realised by aligning the prosthetic foot using number of techniques [6]. In this paper walking asymmetry is evaluated using the inter-leg angle and the step period. An example of asymmetric walking is shown in the schematic diagram in Fig. 1. If both physiological and prosthetic feet have different masses but the same roll-over shape then the kinematic model suggests that the walking is asymmetric. This is shown by the shadowed triangle in Fig.1 describing the asymmetry in terms of the inter-leg angle, as well as the step length.

The proposed mathematical formulation exploits the benefits of passive walking [7-9] and develops an optimal roll-over shape for the prosthetic foot so that the walking is stable and symmetric as shown in Fig. 1b. The mathematical formulation produces an optimal region for roll-over shape gain values that minimises asymmetric walking with respect to both the inter-leg angle (solid curve in Fig. 1c) and the step period (dotted curve in Fig. 1c).

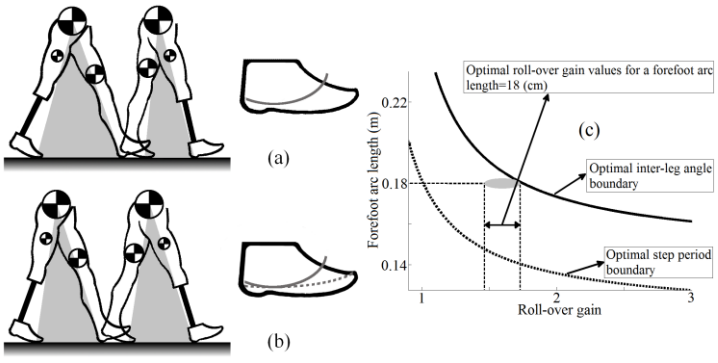

Fig. 1. Walking with identical roll-over shapes (a) and with an optimal roll-over shape (b). The grey region represents the inter-leg angle and the dotted curve shows an optimal roll-over shape. In (c) the solid and dotted lines describe symmetric gait with respect to the inter-leg angle and step period respectively. The ellipsoid shows the range of optimal roll-over gain for a forefoot arc length of 18cm. Refer to the end of Section 3 for further discussion.

Gard et al. [10] studied the kinematics of walking motion and measured the trajectory of a mass as it rolls on a circular arc. It was demonstrated that the trajectory can be modelled by a simple inverted pendulum but with a longer virtual leg length extending to a virtual floor beneath the actual floor. However, even simple double pendulum dynamics is not sufficient to model the biped walking motion. The distances between the rolling contact point and the hip and leg masses change during the rolling motion and must be accurately accounted for in the mathematical formulation.

Mahmoodi et al. [11] gave a detailed review of the applicability of the roll-over shape for a biped walking process and of various computational approaches for modelling biped walking motion. They proposed a mathematical formulation to integrate an arbitrary shaped roll-over shape into a passive walking biped model. However, the formulation was limited in using identical masses for both legs. The proposed formulation, as described in Section 2 and Appendix 1, is designed to study the effect of the mass imbalance on walking symmetry resulting from using a lighter prosthetic foot. Section 2.2 verifies the accuracy of the proposed model by reproducing the circular trajectory of the hip mass as it rolls on a circular arc. It is observed that the actual roll-over shapes are not symmetric around the ankle joint as the forefoot length is always longer than the hindfoot length. The predicted trajectories are shown. Representative anthropometric and prosthetic foot data is used to demonstrate the passive biped walking model and the results are discussed in Section 3. For the physiological foot a roll-over shape is chosen that is consistent with experimentally observed shapes. The multiple pivot point model [11] that describes the roll-over shape is briefly described. The paper is concluded in Section 4.

2. Dynamics of passive walking

The dynamics of the biped walking motion with unbalanced mass is derived from the schematic representation shown in Fig. 2. The effect of a roll-over shape for each leg is modelled as rolling contacts discretised by multiple pivot points where each pivot point is assumed to be a point contact. Mahmoodi et al. [11] should be consulted for a more detailed description of the modelling assumptions and the different phases of the walking motion. The model in this paper is an extension

to that developed by Mahmoodi et al., and only the differences in the model required for asymmetric leg properties will be highlighted.

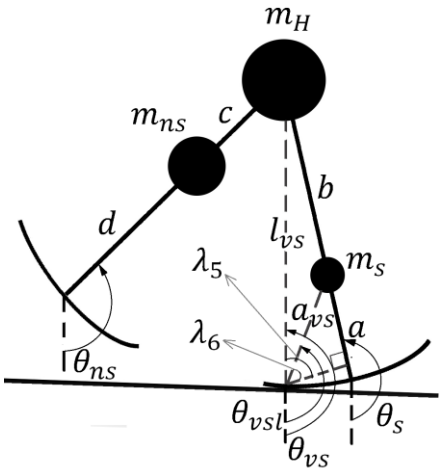

Fig. 2. A schematic representation of a two linked passive biped model with different masses. The dashed lines represent the virtual stance leg (l_{vs}) and the virtual stance lower leg (a_{vs}).

In a multiple pivot point model the dynamics of the walking process during the swing phase and the rolling of the stance leg between every two consecutive pivot points is assumed to be similar to double pendulum dynamics [11]. The initial conditions for each pivot point are changed for every contact point. The supported leg is defined as a link which connects the current pivot point to the hip mass. This virtual leg is different from the actual stance leg (Fig. 2). In this work, the supported leg is called the virtual stance leg (l_{vs}). As the contact moves over the roll-over shape, the virtual stance leg's length, initial angular displacement and initial angular velocity changes and the rolling model needs to capture this change accurately. The rolling contact model proposed by Srinivasan et al. [12] requires position data from gait analysis to calculate joint torques for its active model. Furthermore this model does not allow walking to be asymmetric due to a kinematic invariance assumption, and hence is not considered suitable for the proposed application. McGeer [13] proposed a synthetic wheel and a rimless wheel model for the rolling contact. However, both models assumed negligible weights for the legs and hence the swing leg motion did not have any influence on the dynamics of walking.

The rolling model was later developed for semi-circular feet with hip and leg masses [14]. They assumed that the centres of the semi-circular feet were located on the feet resulting in a symmetric roll-over shape for both sides of the ankle. Some limitations were also reported by the authors with reference to increased foot length at high values of foot radii.

The proposed pivot point model does not constrain the position of the centre of the roll-over shape with the position of point masses. The formulation is generic, and hence, applicable to variety of shapes including non-circular shapes. The approach is designed to predict the positions of masses during the gait cycle using passive dynamics. As a result, the accurate calculation of the virtual stance leg's length, initial angular displacement and initial angular velocity during the rolling motion is necessary and is adequately determined by the proposed pivot point model resulting in an accurate description of the gait as described in Section 2.2. The kinematic model also defines another parameter, referred to as a virtual stance lower leg (a_{vs}), which connects the pivot point to the centre of mass of the stance leg. Its initial conditions are assumed to be identical to those used for the virtual stance leg and hence will change at every time-step.

The equations of motion for every pivot point are similar to the dynamics of the point feet biped [8] but have different positions for the centres of the leg masses and different values of leg masses for the prosthetic and physiological feet. Thus, at the i^{th} pivot point,

$$M^i(\theta)\ddot{\theta} + N^i(\theta,\dot{\theta})\dot{\theta} + g^i(\theta) = 0 \tag{1}$$

where $\theta = [\theta_{vs} \quad \theta_{ns}]^T$ and θ_{vs} and θ_{ns} are measured from the negative *y*-axis, as shown in Fig. 2. This equation is derived from the Lagrangian approach as described in Appendix 1.1.

The inertia matrix, $M(\theta)$, centrifugal terms, $N(\theta,\dot{\theta})$, a vector of gravitational torques, $g(\theta)$, and initial conditions, are

$$M^i(\theta)=\begin{bmatrix} m_s a_{vs}^{i^2}+m_H l_{vs}^{i^2}+m_{ns} l_{vs}^{i^2} & -m_{ns} l_{vs}^i c\cos(\theta_{vs}-\theta_{ns}) \\ -m_{ns} l_{vs}^i c\cos(\theta_{vs}-\theta_{ns}) & m_{ns} c^2 \end{bmatrix} \tag{2}$$

$$N^i(\theta,\dot{\theta})=\begin{bmatrix} 0 & -m_{ns} l_{vs}^i c\dot{\theta}_{ns}\sin(\theta_{vs}-\theta_{ns}) \\ m_{ns} l_{vs}^i c\dot{\theta}_{ns}\sin(\theta_{vs}-\theta_{ns}) & 0 \end{bmatrix} \tag{3}$$

$$g^i(\theta)=\begin{bmatrix} m_s g a_{vs}^i \sin\theta_{vsl}+(m_H g l_{vs}^i+m_{ns} g l_{vs}^i)\sin(\theta_{vs}) \\ -mgc\sin(\theta_{ns}) \end{bmatrix} \tag{4}$$

$$\theta_{vs}^{initial}=\theta_{vs}^i,\quad \theta_{ns}^{initial}=\theta_{ns}^i,\quad \dot{\theta}_{vs}^{initial}=\dot{\theta}_{vs}^i \quad \text{and} \quad \dot{\theta}_{ns}^{initial}=\dot{\theta}_{ns}^i \tag{5}$$

Note that the superscript *i* refers to the *i* th pivot point, and variables and parameters are defined in Fig. 2 and Appendix 1. The equations of motion given by Mahmoodi et al. [11] are recovered if the legs are symmetric.

2.1 Transition phases

The double support transition phase occurs when the body rotates about the last pivot point of the stance leg and the swing leg has just made contact with the ground at its first pivot point. Subsequent to the double support transition phase, a series of stance leg transition phases are defined via the multiple pivot point model. After the first pivot point contacts the ground, the body begins to swing about this contact while the second pivot point contact occurs, which is called as stance leg transition phase. This process continues until the swing leg contacts the ground. The impacts during transition phases are assumed to be inelastic and sliding at the pivot points is not allowed. The mathematical formulation for both phases for unbalance masses is described next.

2.1.1 The double support transition phase

During both transition phases the body configuration remains unchanged and the angular momentum of the whole body is conserved about the impacting pivot points. The angular momentum of the former stance leg about the hip is also conserved during the double support transition phase. The geometry of the body at the first pivot point impact (double support transition phase) leads to the following relationship between the angular position of the virtual stance leg and the swing leg [11]:

$$q_{vs}^{1} + q_{ns}^{1} = -2f + 2p \tag{6}$$

where ϕ is the slope of the ground. The assumption that the body configuration remains unchanged during impact leads to:

$$\theta^{1+} = J\theta^{1-} \tag{7}$$

where

$$J = \begin{bmatrix} 0 & 1 \\ 1 & 0 \end{bmatrix} \tag{8}$$

The superscripts "+" and "-" denote post and pre-pivot point impact variables respectively and the value beside represents the number of pivot points, which for the double support phase is equal to 1. The conservation of angular momentum about the impacting pivot points and the hip, as derived in Appendix 1.2, leads to the condition:

$$\dot{\theta}^{1+} = \frac{H^{1}(\theta)}{H_{d}^{1}}\dot{\theta}^{1-} \tag{9}$$

where the elements of $H^{1}(\theta)$ are

$$\begin{aligned} H_{11}^{1} = {} & m_H m_s b^2 l_{vs}^{e-} l_{vs}^{1+} \cos(\theta_{vs}^{-} - \theta_{vs}^{+}) + m_s^2 b^2 l_{vs}^{1+} a_{vs}^{e-} \cos(\theta_{vs}^{+} - \theta_{vsl}^{-}) \\ & + m_s m_{ns} b^2 l_{vs}^{e-} a_{vs}^{1+} \cos(\theta_{vsl}^{+} - \theta_{vs}^{-}) \\ & - m_s^2 b^2 l_{vs}^{1+} a_{vs}^{e-} \cos(\theta_{ns}^{+} - \theta_{vsl}^{-}) \cos(\theta_{vs}^{+} - \theta_{ns}^{+}) \end{aligned} \tag{10}$$

$$H_{12}^{1} = -m_s m_{ns} b^2 c a_{vs}^{1+} \cos(\theta_{vsl}^{+} - \theta_{ns}^{-}) \tag{11}$$

$$\begin{aligned} H_{21}^{1} = {} & m_s m_H b l_{vs}^{e-} l_{vs}^{1+2} \cos(\theta_{vs}^{+} - \theta_{ns}^{+}) \cos(\theta_{vs}^{-} - \theta_{vs}^{+}) \\ & + m_s^2 b a_{vs}^{e-} l_{vs}^{1+2} \cos(\theta_{vs}^{+} - \theta_{ns}^{+}) \cos(\theta_{vs}^{+} - \theta_{vsl}^{-}) \\ & + m_s m_{ns} b l_{vs}^{e-} l_{vs}^{1+} a_{vs}^{1+} \cos(\theta_{vs}^{+} - \theta_{ns}^{+}) \cos(\theta_{vsl}^{+} - \theta_{vs}^{-}) \\ & - m_s m_H b a_{vs}^{e-} l_{vs}^{1+2} \cos(\theta_{ns}^{+} - \theta_{vsl}^{-}) \\ & - m_s m_{ns} b a_{vs}^{e-} a_{vs}^{1+2} \cos(\theta_{ns}^{+} - \theta_{vsl}^{-}) - m_s^2 b a_{vs}^{e-} l_{vs}^{1+2} \cos(\theta_{ns}^{+} - \theta_{vsl}^{-}) \end{aligned} \tag{12}$$

$$H_{22}^{1} = -m_s m_{ns} b c l_{vs}^{1+} a_{vs}^{1+} \cos(\theta_{vsl}^{+} - \theta_{ns}^{-}) \cos(\theta_{vs}^{+} - \theta_{ns}^{+}) \tag{13}$$

$$H_{d}^{1} = m_s b^2 (m_H l_{vs}^{1+2} + m_s l_{vs}^{1+2} + m_{ns} a_{vs}^{1+2} - m_s l_{vs}^{1+2} \cos^2(\theta_{vs}^{+} - \theta_{ns}^{+})) \tag{14}$$

and *e* represents the *e* th pivot point.

2.1.2 The stance leg transition phase

During a walking step the stance leg transition phase occurs (*e-1)* times from the second pivot point impact up to the eth pivot point. The assumption that the swing leg and the virtual stance leg angle remains unchanged during the impact gives the following condition for the i^{th} pivot point impact $(2 \le i \le e)$:

$$\theta^{i+} = J\theta^{i-} \tag{15}$$

The value of the time-step, t^*, between each pivot point is assumed to be sufficiently small so that the consecutive pivot points accurately define the given roll-over shape. The sensitivity and convergence properties of using different number of pivot points for links with equal masses are discussed in an earlier publication [11]. During the stance leg transition phase the roles of the supported leg and the swing leg remain unchanged and the conservation of angular momentum about the hip during the double support transition phase is replaced with the conservation of angular momentum of the swing leg with respect to hip. The conservation of angular momentum, as derived in Appendix 1.3, leads to the following condition

$$\dot{\theta}^{i+} = \frac{H^i(\theta)}{H_d^i}\dot{\theta}^{i-} \tag{16}$$

where

$$\begin{aligned} H_{11}^i &= m_H l_{vs}^i l_{vs}^{i-1} c\cos(\theta_{vs}^+ - \theta_{vs}^-) + m_s a_{vs}^i a_{vs}^{i-1} c\cos(\theta_{vsl}^+ - \theta_{vsl}^-) \\ &\quad + m_{ns} l_{vs}^i l_{vs}^{i-1} c\cos(\theta_{vs}^+ - \theta_{vs}^-) - m_{ns} l_{vs}^i l_{vs}^{i-1} c\cos(\theta_{vs}^- - \theta_{ns})\cos(\theta_{vs}^+ - \theta_{ns}) \end{aligned} \tag{17}$$

$$H_{12}^i = 0 \tag{18}$$

$$\begin{aligned} H_{21}^i &= (m_H + m_{ns}) l_{vs}^{i\,2} l_{vs}^{i-1}\cos(\theta_{vs}^+ - \theta_{ns})\cos(\theta_{vs}^+ - \theta_{vs}^-) \\ &\quad + m_s l_{vs}^i a_{vs}^i a_{vs}^{i-1}\cos(\theta_{vs}^+ - \theta_{ns})\cos(\theta_{vsl}^+ - \theta_{vsl}^-) \\ &\quad - (m_H + m_{ns}) l_{vs}^{i\,2} l_{vs}^{i-1}\cos(\theta_{vs}^- - \theta_{ns}) - m_s l_{vs}^{i-1} a_{vs}^{i\,2}\cos(\theta_{vs}^- - \theta_{ns}) \end{aligned} \tag{19}$$

Note that $H_{21}^i \to 0$ as the number of pivot points increase.

$$H_{22}^i = H_d^i = m_H l_{vs}^{i\,2} c + m_s a_{vs}^{i\,2} c + m_{ns} l_{vs}^{i\,2} c - m_{ns} l_{vs}^{i\,2} c\cos^2(\theta_{vs}^{i+} - \theta_{ns}^{i+}) \tag{20}$$

2.2 Verification of the model with a trajectory of hip mass rolling on a circular arc

The roll-over shape model proposed in Section 2 was used to model the simple inverted pendulum experiment undertaken by Gard et al. [10] as described in the introduction section. The hip mass was 52.3 kg, the gain value, *r*, was 0.77, and the hindfoot (Arc_h) and forefoot arc (Arc_f) lengths were equal and taken as 11 cm. The trajectory of the hip mass is plotted in Fig. 3a. It is circular as observed by Gard et al. [10]. In contrast, Fig. 3b shows the motion trajectory of the two link model with three point masses, located at the hip joint and at the centres of mass of both legs, corresponding to the mid-person data given by Armstrong [15] (see Table 1). A realistic roll-over shape is used where the hindfoot and forefoot lengths and the gain are $Arc_h = 3\text{cm}, Arc_f = 14\text{cm}$ and $r = 1.5$. The biped is assumed to walk down a shallow slope (2^o) without using any controllers or actuators. The scuffing

problem of the kneeless swing leg with the ground is neglected during the swing phase [7, 13]. The resulting deviation from the circular trajectory is evident in Fig 3b.

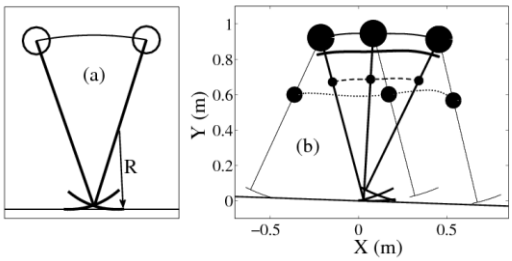

Fig. 3. (a) shows the motion trajectory of a mass rolling on a surface with identical hindfoot and forefoot lengths) (b) describes the motion trajectory two masses located on the stance leg and the swing leg mass. Dotted, dashed and solid lines represent swing leg, stance leg and hip mass respectively. The trajectory of the overall centre of mass is shown with a bold curve.

Table 1. Anthropometric data (mass distribution and the segment lengths) for small, medium and large persons. (*) and (**) present the data were taken from Armstrong (1988) and Chas A Blatchford and Sons Ltd. (2013) respectively.

	Small person	Mid person	Large person
Foot length*	88.4 cm	94.6 cm	100.8 cm
Total mass (m_{total})*	63.3 kg	81.5 kg	97.7 kg
Thigh centre of mass (Thigh COM)*	70.2 cm	75 cm	79.8 cm
Calf centre of mass (Calf COM) *	30.7 cm	33 cm	35.3 cm
Foot centre of mass (Foot COM *	2.6 cm	2.8 cm	3 cm
Thigh mass (m_{thigh})*	7.7 kg	9.8 kg	11.8 kg
Calf mass (m_{calf})*	3.1 kg	3.8 kg	4.5 kg
Foot mass (m_{foot})*	0.8 kg	1 kg	1.1 kg
Physiological lower leg length*	54.9819 cm	59.1233 cm	63.4362 cm
Physiological upper leg length*	33.4181 cm	35.4767 cm	37.3638 cm
Mass ratio $\left(\mu = \frac{m_H}{m_{physiological\ leg}} = \frac{m_{total} - 2\times(m_{thigh}+m_{calf}+m_{foot})}{(m_{thigh}+m_{calf}+m_{foot})}\right)$	3.4569	3.5822	3.6149

Length ratio $\left(\beta = \frac{\text{Physiological upper leg length}}{\text{Physiological lower leg length}}\right)$	0.6078	0.6000	0.5890
Prosthetic lower leg length	62.89 cm	68.67 cm	74.10 cm
Prosthetic upper leg length	25.51 cm	25.93 cm	26.70 cm
Prosthetic lower leg mass (m_{pll})**	1.4 kg	1.4 kg	1.4 kg
Leg's mass ratio $\left(\upsilon = \frac{m_{prosthetideg}}{m_{physiologicalleg}} = \frac{(m_{thigh} + m_{pll})}{(m_{thigh} + m_{calf} + m_{foot})}\right)$	0.7845	0.7671	0.7586
Leg's length ratio $\left(\gamma = \frac{\text{Prosthetic upper leg length}}{\text{Physiological upper leg length}}\right)$	0.7634	0.7309	0.7146

Three parameters, namely the hindfoot arc length (Arc_h), forefoot arc length (Arc_f) and the roll-over gain value, are used to uniquely describe a roll-over shape. The hindfoot arc length and forefoot arc length values present the rear part and the front part of roll-over shape respectively. These lengths are measured from the position of the ankle in relation to the roll-over shape. Note that the ankle position is a point at which the slope of roll-over shape curve is zero. The roll-over shape curve is also aligned so that the corresponding *x* value is zero at this point (Fig. 4). A roll-over gain value (*r*) describes the curvature of the roll-over shape. A higher gain value corresponds to a wider roll-over shape and vice a versa. The polynomial function that describes the roll-over shape [11] is given by:

$$f_R(x) = \frac{1}{r}(x-h)^2 - \frac{1}{r}h^2 \tag{20}$$

where h is defined as the horizontal distance between the origin and the lowest point of the roll-over shape function. For the rest of the analysis in this paper, two roll-over shape curves are used for the physiological leg, as shown in Fig. 4. The corresponding gain values are 1.5 (solid line) and 2.5 (dashed line). Also shown in Fig. 4 are sample roll-over shapes determined from experiments (Sam et al. [24])

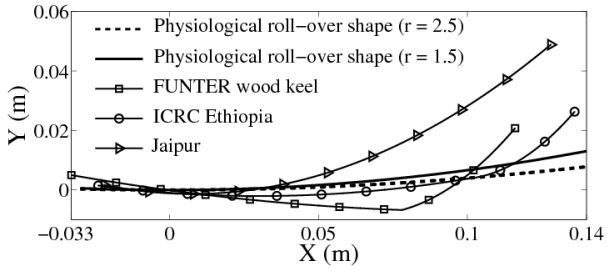

Fig. 4. Three individual roll-over shapes measured by Sam et al. [24]. The solid and dashed lines represent the physiological roll-over shapes used in this paper.

A comparison of the multiple pivot point model with the analytical solution for the rolling motion of a disk on an inclined surface was undertaken by Mahmoodi et al. [11]. It was shown that if the number of pivot points is sufficiently large then the solution given by the multiple pivot point model converges to the analytical displacement profile. The minimum number of pivot points used should be more than 3000 in this example to ensure convergence. This value was also used in all examples presented in this paper.

3. The effect of the prosthetic foot roll-over shape on asymmetric walking

The step length is directly proportional to the inter-leg angle value. Asymmetric walking means that the inter-leg angle (Fig. 5a) and/or step period (Fig. 5e) values are unequal when the prosthetic (dotted curve) and physiological (solid curve) feet act as the supported leg (refer to Fig. 2 and Section 2 for the definition of the supported leg). The inter-leg and step period values are reported to be either larger or smaller when the prosthetic (lighter) foot acts as the supported leg.

Selles et al. [16] argue that even if there is mass imbalance, amputees tend to maintain the same kinematic pattern, i.e. the step length and step period values, by exerting different joint torques. It is also reported in the literature [17-21] that the step length for the prosthetic (lighter foot) stance leg is larger than for the physiological stance leg (e.g. the trend as shown in Fig. 5a) and the prosthetic leg stance period is slightly shorter than for the physiological leg (Fig. 5d). Hekmatfard et al. [22]

tabulated the step length variation with respect to additional mass placed on the prosthetic foot. Initially, the prosthetic foot step length [53.4 (±9.8) cm] was higher than the physiological foot [52.6 (±9.2) cm]. However, as 600g was added to the knee of the prosthetic foot the step length for the prosthetic foot [50.2 (±8.1) cm] became smaller than the physiological foot [54.8 (±11.2) cm]. When 300g was added at both the knee and ankle of the prosthetic foot the step period became almost same for both prosthetic and physiological feet [53.5 and 53.1 cm respectively]. The gait cycle duration almost remained the same for all combinations.

The active model proposed by Srinivasan et al. [12] may not be the best option to gain insight into such behaviour as amputees will adjust joint torques to maintain kinematic invariance. The proposed mathematical formulation, based on passive dynamics, may offer some insight. The observations reported in the literature depend on the actual roll-over shapes used and the corresponding anthropometric data of the amputee is unknown. However, for a given leg mass ratio $(\nu = 0.77)$ and leg length ratio $(\gamma = 0.73)$, as defined in Table 1 for the mid person, and shown as section AA in Figs. 5a and d**,** the results from the proposed mathematical model suggest that the inter-leg angle for a lighter prosthetic foot is larger than the physiological foot. For the same mass ratio, if the leg length ratio is increased, i.e. the position of the centre of mass on the prosthetic foot is lowered, then the kinematic modelling suggests a tendency for symmetric walking **(**Fig. 5a). The trend reverses for γ values greater than 0.87. This concurs with the observations made by Hekmatfard et al. [22] on step length variation. Similarly, Fig. 5d illustrates that the walking is symmetric with respect to step period until γ = 0.82. If the prosthetic foot roll-over shape is optimised with respect to inter-leg angle then the walking can be made symmetric for γ = 0.73 (Fig. 5b), however, it remains asymmetric with respect to step period (Fig. 5 e). Fig 5 f demonstrates that if the prosthetic foot roll-over shapes are optimised with reference to step period then inter-leg angle remains asymmetric (Fig 5c). For this example, the forefoot arc length $\left(Arc_f^{\alpha} = Arc_f^{T}\right)$ was arbitrarily chosen to be 17cm in order to determine the corresponding optimal gain values. The gain values were found to be $r^{\alpha} = 2.27$ (Figs.

5b and e) and $r^T = 1.1$ (Fig. 5c and f), where the superscript α or T denotes optimal prosthetic roll-over parameters with respect to the inter-leg angle or the step period respectively.

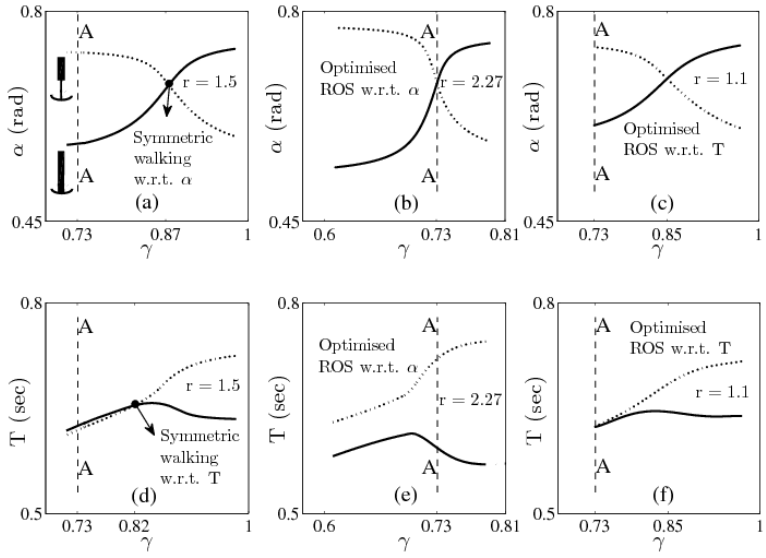

Fig. 5. Asymmetry diagrams for inter-leg angle (a, b, c) and step period (d, e, f). The solid and dotted curves correspond to gait parameters when the physiological leg and the prosthetic leg act as the supported leg respectively (refer to Fig. 2 and Section 2 for the definition of supported leg). The dashed line A-A represents the leg's length ratio of a mid person as described in Table 1. The point of intersection in each figure represents symmetric walking either with reference to inter-leg angle or the step period. The plots (a,d) correspond identical roll-over gain value (r=1.5) for both legs. The optimal roll-over gain value (r=2.27 and r=1.1) with respect to the inter-leg angle and step period value respectively in plots (b,e) and (c,f). Optimal gain value means either the inter-leg angle value is same for both legs (Section A-A in plot b) or the step period value (Section A-A in plot f) is identical.

It should be noted that for the same shoe size or foot length, the roll-over shape arc lengths for both feet do not have to be same. Hence, the forefoot arc length values for the prosthetic foot can differ from the physiological leg value and both values will be less than the corresponding shoe size of the amputee [23, 24].

The locus of intersection points that signify the symmetry, as defined in Figs. 5b and f, is plotted in Fig. 6c for various forefoot arc length and gain values. The solid curves in Fig. 6 correspond to symmetry with respect to inter-leg angle and the dotted curves represent symmetry with respect to step period. For Figs. 6a, c and e, the input roll-over shape for the physiological leg has values

$Arc_h = 3\text{cm}, Arc_f = 14\text{cm}$ and $r = 1.5$, whereas the gain value r is changed to 2.5 for Figs. 6b, d and f. Fig. 6 shows that the higher prosthetic foot roll-over gain values (i.e. increasing the stiffness of the prosthetic foot) are associated with smaller prosthetic forefoot arc lengths for symmetric walking. Comparison of Figs. 6a, c and e with Figs. 6b, d and f highlights that a higher physiological foot roll-over gain also requires a higher prosthetic forefoot arc length. Also, for a given physiological roll-over shape, the anthropometric data with reference to the small (Figs. 6a, b), mid (Figs. 6c, d) or large (Figs. 6e, f) person does not influence the prosthetic foot roll-over shape parameters for symmetric walking with reference to the step period (dotted curves in Fig. 6 are same for Figs. 6a, c and e, as well as Figs. 6b, d, and f) whereas the optimum curve with respect to inter-leg angle is significantly different. The shorter curves shown in Figs. 6b, d, and f arise because of the non-existence of symmetric walking solutions for the assumed anthropometric and roll-over shape data.

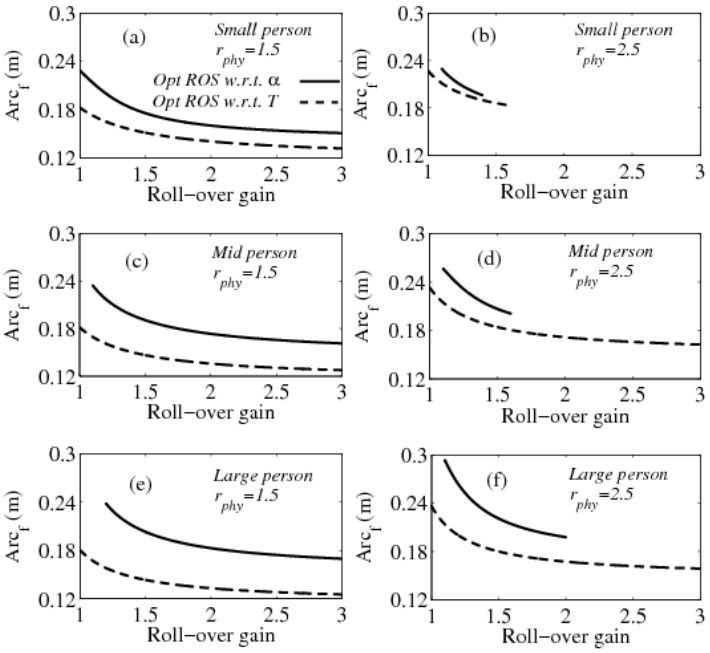

Fig. 6. The locus of points of intersection that represent the symmetry, as illustrated in Fig 5 b and f, is shown for small (a, b), medium (c, d) and large (e, f) persons. The schematic diagram shown in Fig. 1c is based on Fig 6 c. The solid and dashed curves represent the optimal roll-over parameters with respect to the inter-leg angle and the step period respectively. The first and second columns show the optimal relationship for small, mid and large body while the physiological roll-over gain is 1.5 and 2.5 respectively.

The effect of the optimised roll-over shape, with respect to the inter-leg angle and the step period, on the angular velocity and angular displacement variation with respect to time (Fig. 7) is studied to gain further insight into the asymmetry caused by the unbalanced mass distributions of both feet. The physiological roll-over shape gain, hindfoot arc length and forefoot arc length values are 1.5, 3cm and 14cm respectively and the leg mass ratio and leg length ratio correspond to the mid person with prosthetic leg ($\nu = 0.77$ and $\gamma = 0.73$). For a prosthetic foot gain value of 1.2 (Fig. 6c), the optimal forefoot arc length values with reference to inter-leg angle and step period are $Arc_f^{\alpha} = 21.5\,\text{cm}$ and $Arc_f^{T} = 16\,\text{cm}$ respectively.

The curve 1-2 in Fig. 7c (dotted curve) denotes the swing phase of the prosthetic foot followed by the double support phase (2-3). In the subsequent stage (3-4) the prosthetic foot acts as a stance leg and the next double support phase (4-1) completes the gait cycle. Similarly, the solid curve (Figs. 7a and b) shows the variation for the physiological leg. Figs. 7a and b show the variation when the roll-over shapes are optimised for step period and inter-leg angles respectively, corresponding to the dotted line and solid curves shown in Fig. 6. Fig. 7b illustrates that the angular velocity and angular displacement variations for both prosthetic and physiological feet are similar when the prosthetic foot's roll-over shape is optimised with reference to inter-leg angle. This was not observed when the roll-over shape was optimised with reference to the step period (Fig. 7a). The change in the angular velocity during the double support phase (2-3) for the prosthetic foot is much longer than the physiological foot as shown in Fig. 7a (dotted line). This signifies residual walking asymmetry even though the prosthetic foot's roll-over shape is optimised with reference to the step period. There is minimal residual asymmetry for inter-leg angle based optimisation (Fig. 7b). Hence, the optimal elliptical region defined in Fig. 1 is shown closer to the inter-leg angle curve.

Future work will consider the location of the hip, knee and ankle at various walking speeds [25], in addition to the step lengths and inter-leg angles, and study the effect of using optimal roll-overs shapes. Li and Yang [26] studied the emergence of the chaotic gait for a simple point foot model. It will be interesting to see the effect of roll-over shapes on the basin of attraction and chaotic gait.

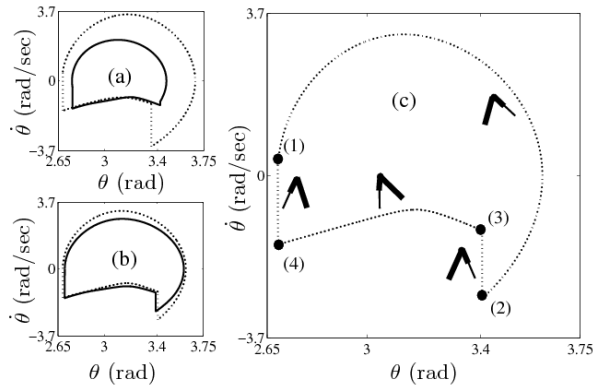

Fig. 7. The relationship between the angular velocity and angular displacement is shown for both physiological (as shown by solid curves in a and b) and prosthetic foot (dotted curve). Steps 1-2-3-4-1 in Figure c demonstrate a gait cycle with the swing phase for the prosthetic foot, double support phase, prosthetic foot as a stance leg and the subsequent double support phase respectively. Figures (a) and (b) are shown for optimised roll-over shapes for the prosthetic foot with reference to step period (a) and inter-leg angle (b). The similarity of curves within each plot is considered as another measure of symmetry. Figure (b) is considered as more symmetric and hence, the ellipsoid shown in Fig. 1c is chosen closer to the inter-leg angle curve.

4. Conclusion

Roll-over shapes have been used in the literature to characterise the direction of the ground reaction with reference to the position of the ankle-knee part of the leg. The roll-over shape of a prosthetic foot can be adjusted by varying the stiffness of the foot. The proposed passive walking kinematic model does not require information on joint torques, and hence does not need the motion or natural gait analysis of an amputee which is often unavailable. The model quantifies the natural tendency for asymmetry resulting from the mass unbalance, in terms of both the inter-leg angle and the step period, so that the necessary corrective action required at the prosthetic foot is measured by predicting an optimal prosthetic foot roll-over shape. The sensitivity of the roll-over shape with the stability and symmetry of the walking process in terms of the inter-leg angle and step period is assessed in order to discover optimal regions with reference to forefoot arc length and the roll-over shape gain that quantifies the stiffness profile of the prosthetic foot.

Appendix 1: Mathematical derivations

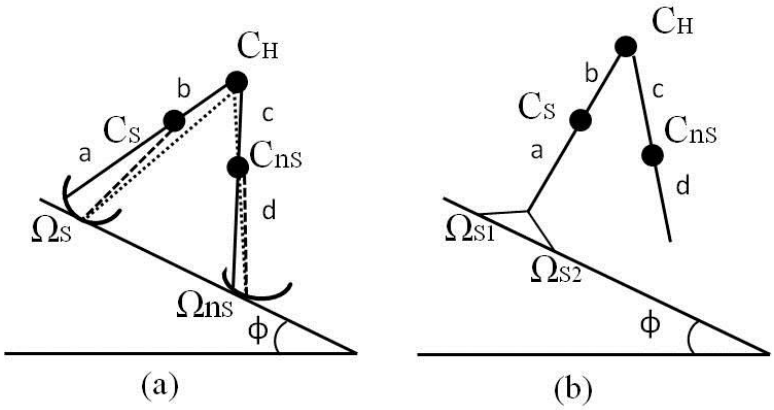

Fig. 8. Schematic representation of the positions of hip mass (C_H), supported and non-supported legs mass (C_s and C_{ns}). Ω_s and Ω_{ns} are the points of contact of the support and non-support legs. Dotted lines denote the virtual lengths of corresponding masses. (a) illustrates a double support phase and a schematic model of pivot point contacts for the swing phase is shown in (b).

Appendix 1.1

Derivation of Equation 1 ($M^i(\theta)\ddot{\theta}+N^i(\theta,\dot{\theta})\dot{\theta}+g^i(\theta)=0$) using an Euler Langrangian approach for the single support phase

$$\frac{d}{dt}\left(\frac{\partial L^i(\theta,\dot{\theta})}{\partial\dot{\theta}}\right)-\frac{\partial L^i(\theta,\dot{\theta})}{\partial\theta}=0,\quad L^i(\theta,\dot{\theta})=K^i(\theta,\dot{\theta})-P^i(\theta) \tag{A.1}$$

$$K^i(\theta,\dot{\theta})=\frac{1}{2}m_H\|\vec{v}_H\|^2+\frac{1}{2}m_s\|\vec{v}_s\|^2+\frac{1}{2}m_{ns}\|\vec{v}_{ns}\|^2 \tag{A.2}$$

$$P^i(\theta)=-m_H g l^i_{vs}\cos\theta_{vs}-m_s g a^i_{vs}\cos\theta_{vsl}-m_{ns}g\left(l^i_{vs}\cos\theta_{vs}-c\cos\theta_{ns}\right) \tag{A.3}$$

$$\overrightarrow{v_H}=l_{vs}\dot{\theta}_s\cos\theta_{vs}\vec{i}+l_{vs}\dot{\theta}_s\sin\theta_{vs}\vec{j} \tag{A.4}$$

$$\vec{v}_s=a_{vs}\dot{\theta}_s\cos\theta_{vsl}\vec{i}+a_{vs}\dot{\theta}_s\sin\theta_{vsl}\vec{j} \tag{A.5}$$

$$\overrightarrow{v_{ns}}=\left(l_{vs}\dot{\theta}_s\cos\theta_{vs}-c\dot{\theta}_{ns}\cos\theta_{ns}\right)\vec{i}+\left(l_{vs}\dot{\theta}_s\sin\theta_{vs}-c\dot{\theta}_{ns}\sin\theta_{ns}\right)\vec{j} \tag{A.6}$$

Appendix 1.2:

Derivation of the Equation 9 ($\dot{\theta}^{1+}=\frac{H^1(\theta)}{H^1_d}\dot{\theta}^{1-}$) for the double support transition phase:

The condition of conservation of angular momentum about impacting pivot points and hip (Fig 8a) leads to:

$$m_H\overrightarrow{\Omega_{ns}^{-}C_H}\wedge\overrightarrow{v_H^{-}}+m_s\overrightarrow{\Omega_{ns}^{-}C_s^{-}}\wedge\overrightarrow{v_s^{-}}+m_{ns}\overrightarrow{\Omega_{ns}^{-}C_{ns}^{-}}\wedge\overrightarrow{v_{ns}^{-}}= m_H\overrightarrow{\Omega_s^{+}C_H}\wedge\overrightarrow{v_H^{+}}+m_{ns}\overrightarrow{\Omega_s^{+}C_s^{+}}\wedge\overrightarrow{v_s^{+}}+m_s\overrightarrow{\Omega_s^{+}C_{ns}^{+}}\wedge\overrightarrow{v_{ns}^{+}} \quad \text{(A.7)}$$

$$m_s\overrightarrow{C_HC_s^{-}}\wedge\overrightarrow{v_s^{-}}=m_s\overrightarrow{C_HC_{ns}^{+}}\wedge\overrightarrow{v_{ns}^{+}} \quad \text{(A.8)}$$

$$\dot{\theta}_s=\dot{\theta}_{vs}=\dot{\theta}_{vsl} \quad \text{(A.9)}$$

$$\overrightarrow{\Omega_{ns}^{-}C_H}=l_{vs}^{1+}\sin\theta_{vs}^{+}\vec{i}-l_{vs}^{1+}\cos\theta_{vs}^{+}\vec{j} \quad \text{(A.10)}$$

$$\overrightarrow{v_H^{-}}=l_{vs}^{e-}\dot{\theta}_s^{-}\cos\theta_{vs}^{-}\vec{i}+l_{vs}^{e-}\dot{\theta}_s^{-}\sin\theta_{vs}^{-}\vec{j} \quad \text{(A.11)}$$

$$\overrightarrow{\Omega_{ns}^{-}C_s^{-}}=\left(l_{vs}^{1+}\sin\theta_{vs}^{+}-b\sin\theta_{ns}^{+}\right)\vec{i}+\left(-l_{vs}^{1+}\cos\theta_{vs}^{+}+b\cos\theta_{ns}^{+}\right)\vec{j} \quad \text{(A.12)}$$

$$\overrightarrow{v_s^{-}}=a_{vs}^{e-}\dot{\theta}_s^{-}\cos\theta_{vsl}^{-}\vec{i}+a_{vs}^{e-}\dot{\theta}_s^{-}\sin\theta_{vsl}^{-}\vec{j} \quad \text{(A.13)}$$

$$\overrightarrow{\Omega_{ns}^{-}C_{ns}^{-}}=a_{vs}^{1+}\sin\theta_{vsl}^{+}\vec{i}-a_{vs}^{1+}\cos\theta_{vsl}^{+}\vec{j} \quad \text{(A.14)}$$

$$\overrightarrow{v_{ns}^{-}}=\left(l_{vs}^{e-}\dot{\theta}_s^{-}\cos\theta_{vs}^{-}-c\dot{\theta}_{ns}^{-}\cos\theta_{ns}^{-}\right)\vec{i}+\left(l_{vs}^{e-}\dot{\theta}_s^{-}\sin\theta_{vs}^{-}-c\dot{\theta}_{ns}^{-}\sin\theta_{ns}^{-}\right)\vec{j} \quad \text{(A.15)}$$

$$\overrightarrow{\Omega_s^{+}C_H}=l_{vs}^{1+}\sin\theta_{vs}^{+}\vec{i}-l_{vs}^{1+}\cos\theta_{vs}^{+}\vec{j} \quad \text{(A.16)}$$

$$\overrightarrow{v_H^{+}}=l_{vs}^{1+}\dot{\theta}_s^{+}\cos\theta_{vs}^{+}\vec{i}+l_{vs}^{1+}\dot{\theta}_s^{+}\sin\theta_{vs}^{+}\vec{j} \quad \text{(A.17)}$$

$$\overrightarrow{\Omega_s^{+}C_s^{+}}=a_{vs}^{1+}\sin\theta_{vsl}^{+}\vec{i}-a_{vs}^{1+}\cos\theta_{vsl}^{+}\vec{j} \quad \text{(A.18)}$$

$$\overrightarrow{v_s^{+}}=a_{vs}^{1+}\dot{\theta}_s^{+}\cos\theta_{vsl}^{+}\vec{i}+a_{vs}^{1+}\dot{\theta}_s^{+}\sin\theta_{vsl}^{+}\vec{j} \quad \text{(A.19)}$$

$$\overrightarrow{\Omega_s^{+}C_{ns}^{+}}=\left(l_{vs}^{1+}\sin\theta_{vs}^{+}-b\sin\theta_{ns}^{+}\right)\vec{i}+\left(-l_{vs}^{1+}\cos\theta_{vs}^{+}+b\cos\theta_{ns}^{+}\right)\vec{j} \quad \text{(A.20)}$$

$$\overrightarrow{v_{ns}^{+}}=\left(l_{vs}^{1+}\dot{\theta}_s^{+}\cos\theta_{vs}^{+}-b\dot{\theta}_{ns}^{+}\cos\theta_{ns}^{+}\right)\vec{i}+\left(l_{vs}^{1+}\dot{\theta}_s^{+}\sin\theta_{vs}^{+}-b\dot{\theta}_{ns}^{+}\sin\theta_{ns}^{+}\right)\vec{j} \quad \text{(A.21)}$$

$$\overrightarrow{C_HC_s^{-}}=-b\sin\theta_{ns}^{+}\vec{i}+b\cos\theta_{ns}^{+}\vec{j} \quad \text{(A.22)}$$

$$\overrightarrow{C_HC_{ns}^{+}}=-b\sin\theta_{ns}^{+}\vec{i}+b\cos\theta_{ns}^{+}\vec{j} \quad \text{(A.23)}$$

Substituting these equations in A.7 and A.8 leads to the Equation 9.

Appendix 1.3:

Derivation of Equation 16 ($\dot{\theta}^{i+} = \frac{H^i(\theta)}{H_d^i}\dot{\theta}^{i-}$) for the stance leg transition phase

The condition of conservation of angular momentum about impacting pivot points and hip (Fig 8b) leads to:

$$m_H \overrightarrow{\Omega_{s2}C_H} \wedge \overrightarrow{v_H^-} + m_s \overrightarrow{\Omega_{s2}C_s} \wedge \overrightarrow{v_s^-} + m_{ns} \overrightarrow{\Omega_{s2}C_{ns}} \wedge \overrightarrow{v_{ns}^-} = m_H \overrightarrow{\Omega_{s2}C_H} \wedge \overrightarrow{v_H^+} + m_s \overrightarrow{\Omega_{s2}C_s} \wedge \overrightarrow{v_s^+} + m_{ns} \overrightarrow{\Omega_{s2}C_{ns}} \wedge \overrightarrow{v_{ns}^+} \quad \text{(A.24)}$$

$$m_{ns} \overrightarrow{C_H C_{ns}} \wedge \overrightarrow{v_{ns}^-} = m_{ns} \overrightarrow{C_H C_{ns}} \wedge \overrightarrow{v_{ns}^+} \quad \text{(A.25)}$$

$$\overrightarrow{\Omega_{s2}C_H} = l_{vs}^i \sin\theta_{vs}^+ \vec{i} - l_{vs}^i \cos\theta_{vs}^+ \vec{j} \quad \text{(A.26)}$$

$$\overrightarrow{v_H^-} = l_{vs}^{i-1}\dot{\theta}_s^- \cos\theta_{vs}^- \vec{i} + l_{vs}^{i-1}\dot{\theta}_s^- \sin\theta_{vs}^- \vec{j} \quad \text{(A.27)}$$

$$\overrightarrow{\Omega_{s2}C_s} = a_{vs}^i \sin\theta_{vs}^+ \vec{i} - a_{vs}^i \cos\theta_{vs}^+ \vec{j} \quad \text{(A.28)}$$

$$\overrightarrow{v_s^-} = a_{vs}^{i-1}\dot{\theta}_s^- \cos\theta_{vsl}^- \vec{i} + a_{vs}^{i-1}\dot{\theta}_s^- \sin\theta_{vsl}^- \vec{j} \quad \text{(A.29)}$$

$$\overrightarrow{\Omega_{s2}C_{ns}} = \left(l_{vs}^i \sin\theta_{vs}^+ - c\sin\theta_{ns}\right)\vec{i} + \left(-l_{vs}^i \cos\theta_{vs}^+ + c\cos\theta_{ns}\right)\vec{j} \quad \text{(A.30)}$$

$$\overrightarrow{v_{ns}^-} = \left(l_{vs}^{i-1}\dot{\theta}_s^- \cos\theta_{vs}^- - c\dot{\theta}_{ns}^- \cos\theta_{ns}\right)\vec{i} + \left(l_{vs}^{i-1}\dot{\theta}_s^- \sin\theta_{vs}^- - c\dot{\theta}_{ns}^- \sin\theta_{ns}\right)\vec{j} \quad \text{(A.31)}$$

$$\overrightarrow{v_H^+} = l_{vs}^i \dot{\theta}_s^+ \cos\theta_{vs}^+ \vec{i} + l_{vs}^i \dot{\theta}_s^+ \sin\theta_{vs}^+ \vec{j} \quad \text{(A.32)}$$

$$\overrightarrow{v_s^+} = a_{vs}^i \dot{\theta}_s^+ \cos\theta_{vsl}^+ \vec{i} + a_{vs}^i \dot{\theta}_s^+ \sin\theta_{vsl}^+ \vec{j} \quad \text{(A.33)}$$

$$\overrightarrow{v_{ns}^+} = \left(l_{vs}^i \dot{\theta}_s^+ \cos\theta_{vs}^+ - c\dot{\theta}_{ns}^+ \cos\theta_{ns}\right)\vec{i} + \left(l_{vs}^i \dot{\theta}_s^+ \sin\theta_{vs}^+ - c\dot{\theta}_{ns}^+ \sin\theta_{ns}\right)\vec{j} \quad \text{(A.34)}$$

$$\overrightarrow{C_H C_{ns}} = -c\sin\theta_{ns}\vec{i} + c\cos\theta_{ns}\vec{j} \quad \text{(A.35)}$$

Substituting these equations in A.24 and A.25 leads to the Equation 16.

References

[1] Y. Sagawa Jr, K. Turcot, S. Armand, A. Thevenon, N. Vuillerme, E. Watelain, Biomechanics and physiological parameters during gait in lower-limb amputees: A systematic review, Gait & Posture, 33 (2011) 511-526.

[2] H. Van der Linde, C.J. Hofstad, A.C. Geurts, K. Postema, J.H. Geertzen, J. van Limbeek, A systematic literature review of the effect of different prosthetic components on human functioning with a lower-limb prosthesis, J Rehabil Res Dev, 41 (2004) 555-570.

[3] A.H. Hansen, D.S. Childress, Investigations of roll-over shape: implications for design, alignment, and evaluation of ankle-foot prostheses and orthoses, Disability Rehabilitation, 32 (2010) 2201-2209.

[4] L. Ren, D. Howard, L. Ren, C. Nester, L. Tian, A generic analytical foot rollover model for predicting translational ankle kinematics in gait simulation studies, Journal of Biomechanics, 43 (2010) 194-202.
[5] C.C. Wang, A.H. Hansen, Response of able-bodied persons to changes in shoe rocker radius during walking: Changes in ankle kinematics to maintain a consistent roll-over shape, Journal of Biomechanics, 43 (2010) 2288-2293.
[6] A.H. Hansen, M.R. Meier, M. Sam, D.S. Childress, M.L. Edwards, Alignment of trans-tibial prostheses based on roll-over shape principles, Prosthetics and Orthotics International, 27 (2003) 89-99.
[7] M. Garcia, A. Chatterjee, A. Ruina, M. Coleman, The simplest walking model: stability, complexity, and scaling, J Biomech Eng, 120 (1998) 281-288.
[8] A. Goswami, B. Thuilot, B. Espiau, A Study of the Passive Gait of a Compass-Like Biped Robot: Symmetry and Chaos, The International Journal of Robotics Research, 17 (1998) 1282-1301.
[9] M.J. Kurz, T.N. Judkins, C. Arellano, M. Scott-Pandorf, A passive dynamic walking robot that has a deterministic nonlinear gait, Journal of Biomechanics, 41 (2008) 1310-1316.
[10] S.A. Gard, D.S. Childress, What Determines the Vertical Displacement of the Body During Normal Walking?, J Prosthet Orthot, 13 (2001) 64-67.
[11] P. Mahmoodi, R.S. Ransing, M.I. Friswell, Modelling the effect of 'heel to toe' roll-over contact on the walking dynamics of passive biped robots, Applied Mathematical Modelling, 37 (2013) 7352-7373.
[12] S. Srinivasan, E.R. Westervelt, A.H. Hansen, A Low-Dimensional Sagittal-Plane Forward-Dynamic Model for Asymmetric Gait and Its Application to Study the Gait of Transtibial Prosthesis Users, Journal of Biomechanical Engineering, 131 (2009) 031003.
[13] T. McGeer, Passive Dynamic Walking, The International Journal of Robotics Research, 9 (1990) 62-82.
[14] F. Asano, L. Zhi-Wei, On Energy-Efficient and High-Speed Dynamic Biped Locomotion with Semicircular Feet, in: Intelligent Robots and Systems, 2006 IEEE/RSJ International Conference on, 2006, pp. 5901-5906.
[15] H.G. Armstrong Anthropometry and Mass Distribution for Human Analogues, in, 1988.
[16] R.W. Selles, J.B. Bussmann, L.M. Klip, B. Speet, A.J. Van Soest, H.J. Stam, Adaptations to mass perturbations in transtibial amputees: Kinetic or kinematic invariance?, Archives of Physical Medicine and Rehabilitation, 85 (2004) 2046-2052.
[17] E. Isakov, O. Keren, N. Benjuya, Trans–tibial amputee gait: Time–distance parameters and EMG activity, Prosthetics and Orthotics International, 24 (2000) 216-220.
[18] N. Mizuno, T. Aoyama, A. Nakajima, T. Kasahara, K. Takami, Functional evaluation by gait analysis of various ankle-foot assemblies used by below-knee amputees, Prosthet Orthot Int, 16 (1992) 174-182.
[19] J.L. Robinson, G.L. Smidt, J.S. Arora, Accelerographic, temporal, and distance gait factors in below-knee amputees, Phys Ther, 57 (1977) 898-904.
[20] H.B. Skinner, R.L. Barrack, Ankle weighting effect on gait in able-bodied adults, Archives of Physical Medicine and Rehabilitation, 71 (1990) 112-115.
[21] J.D. Smith, P.E. Martin, Walking patterns change rapidly following asymmetrical lower extremity loading, Human Movement Science, 26 (2007) 412-425.
[22] M. Hekmatfard, F. Farahmand, I. Ebrahimi, Effects of prosthetic mass distribution on the spatiotemporal characteristics and knee kinematics of transfemoral amputee locomotion, Gait & Posture, 37 (2013) 78-81.
[23] C. Curtze, A.L. Hof, H.G. van Keeken, J.P.K. Halbertsma, K. Postema, B. Otten, Comparative roll-over analysis of prosthetic feet, Journal of Biomechanics, 42 (2009) 1746-1753.
[24] M. Sam, A.H. Hansen, D.S. Childress, Characterisation of prosthetic feet used in low-income countries, Prosthetics and Orthotics International, 28 (2004) 132-140.
[25] H. Richter, D. Simon, W. A Smith and S. Samorezov, Dynamic modelling, parameter estimation and control of a leg prosthesis test robot, Applied Mathematical Modelling, 39, 2, (2015), 559-573
[26] Q. Li, X-S Yang, New walking dynamics in the simplest passive bipedal walking model, Applied Mathematical Modelling, 36, 11, (2012), 5262-5271